Anomalous exciton–radiation coupling in the nano-to-bulk crossover regime

2007 J. Phys.: Condens. Matter 19 445008

(http://iopscience.iop.org/0953-8984/19/44/445008)

IOP PUBLISHING JOURNAL OF PHYSICS: CONDENSED MATTER

J. Phys.: Condens. Matter **19** (2007) 445008 (20pp) doi:10.1088/0953-8984/19/44/445008

Anomalous exciton–radiation coupling in the nano-to-bulk crossover regime

H Ishihara[1,2], A Syouji[3], Y Segawa[4] and M Bamba[5]

[1] Department of Physics and Electronics, Osaka Prefecture University, Sakai, Osaka 599-8531, Japan
[2] CREST, Japan Science and Technology Agency, Kawaguchi, Saitama 332-0012, Japan
[3] KARC, National Institute of Information and Communications Technology, Kobe, Hyogo 651-2492, Japan
[4] Exciton Engineering Laboratory, The Institute of Physical and Chemical Research, RIKEN, Wako, Saitama 351-0198, Japan
[5] Department of Materials Engineering Science, Osaka University, Toyonaka, Osaka 560-8531, Japan

E-mail: ishi@pe.osakafu-u.ac.jp

Received 3 December 2006, in final form 13 March 2007
Published 18 October 2007
Online at stacks.iop.org/JPhysCM/19/445008

Abstract

Anomalous exciton–radiation coupling in the sample-size regime beyond the long-wavelength approximation (LWA) is discussed. In high-quality samples fabricated using the latest technologies, the long-range excitonic coherence and non-LWA effect cause a peculiar interplay between the spatial structures of the radiation and excitonic waves, which emerge as an anomalous level structure of the exciton–radiation coupled system including an extremely large radiative correction. We theoretically demonstrated such a situation for a thin film by a microscopic nonlocal theory in which a size-resonant enhancement of the radiative damping constant and successive interchanges of the confined polariton states can be observed. In order to verify the predicted level structure of confined polaritons, we present the results of non-degenerate two-photon scattering spectroscopy investigations and a corresponding analysis based on the nonlocal theory for the second-order nonlinear process. This scheme has successfully elucidated peculiar level structures of confined polaritons in the non-LWA regime. In the last half of the paper, a new type of resonant hyper-parametric scattering (RHPS) spectroscopy with a non-degenerate induced excitation is theoretically proposed as another method to study confined polaritons in the non-LWA regime. Some calculations for thin films are demonstrated to reveal the potentiality of this method that provides rich information on confined biexcitons and polaritons.

(Some figures in this article are in colour only in the electronic version)

1. Introduction

1.1. Background

One of the interesting features of optical responses in nanostructures is their dependence on the type of sample structure. In particular, the size dependence arising from the coherence of confined excitons is highly attractive because it provides information on quantum structures of confined systems and the possible mechanisms for novel photo-functions. In a strong confinement regime, the electron and hole are individually confined, and the wavefunction of their relative motion shrinks. This effect leads to an increase in the transition dipole moment, which increases the radiative coupling strength [1, 2]. On the other hand, in a weak coupling regime, the centre-of-mass (c.m.) motion of an exciton is confined; the dipole moment is size-linearly enhanced as long as the c.m. wavefunction is coherent over the entire sample [3, 4]. The origin of this effect is basically the same as that of the giant-oscillator-strength effect of the bound exciton [5, 6]. In both cases, the size dependence of the exciton–radiation coupling is described in terms of the size-dependent oscillator strength obtained under the long-wavelength approximation (LWA). The size-linear enhancement of the oscillator strength has been experimentally observed through the same behaviour of the radiative decay rate and third-order nonlinear responses of comparatively small quantum dots [8–10]. Another typical confinement effect described in the LWA is a selection rule of optical transition. For example, a clear selection rule has been observed for CuCl thin films by Tang *et al* [7], where dips in linear transmissions are observed only for even parity of states for thicknesses from 10 nm to 16 nm. The wavelength of light resonant with excitonic states is normally much longer than the coherent volume of their wavefunctions; hence, in this way, the LWA has successfully described the size-dependent optical responses of nanostructures.

However, it should be noted that in high-quality samples, there is a possibility of the coherent length of excitonic c.m. motion increasing considerably, thereby invalidating the LWA. This situation is often realized particularly in film-type samples because inhomogeneity is well suppressed in comparison with the other geometries, and the excitonic coherence can be well maintained. Such a long coherence has been observed for a long time as exciton–polariton interference in thin films. In the case of thicker films, Kielev *et al* [11] observed a polariton interference in CdSe by using one-photon spectroscopy, and similar interference spectra were observed in a CuCl thin film by Mita *et al* [12]. Further, the complicated spectral structures due to these interferences have been theoretically explained [13–15]. However, the complex correlation between the spectral structures and quantum states was not completely elucidated by these studies.

After these studies on polariton interference, the resonant behaviour of the internal electromagnetic (EM) field was identified as a source of the size-dependent nonlinear response [16]. Although we can regard the resonant behaviour of the internal EM field as another feature of polariton interference, it has a new potential to cause drastic enhancement of the nonlinear response in the non-LWA regime. This possibility has been theoretically observed [17, 18], and here, the spatial structure of the internal EM field plays an essential role.

When the excitonic c.m. motion is allowed, the optical response is generally nonlocal; namely, the induced polarization at a position $\boldsymbol{r}$, in the linear response for example, is written in a nonlocal form, i.e.,

$$\boldsymbol{P}(\boldsymbol{r}) = \int \chi(\boldsymbol{r}, \boldsymbol{r}')\boldsymbol{E}(\boldsymbol{r}')\,\mathrm{d}\boldsymbol{r}', \tag{1}$$

where χ is the linear susceptibility, and $\boldsymbol{E}(\boldsymbol{r})$ is the electric field at position $\boldsymbol{r}$. The coupled

system of this equation and the microscopic Maxwell equation determines the motions of the induced polarization and the internal EM field self-consistently. As a result, the internal field shows a nanoscale spatial structure. According to the condition of the incident frequency and the system size, a particular spatial pattern of the internal EM field is enhanced by the nanoscale Fabry–Perot effect [18]. This causes a drastic breakdown of the LWA and an anomalous size dependence of the nonlinear response [18, 19]. The predicted size-resonant enhancement of the nonlinear response from the non-dipole-type excitonic state has been experimentally verified by using GaAs thin layers [20, 21]. Further, non-monotonic thickness dependence of the excitonic radiative decay constant has been observed for the same excitonic state [22]; this is in contrast with the size-linear enhancement of the oscillator strength.

1.2. Recent studies on the exciton–radiation coupling in the non-LWA regime

In order to obtain a comprehensive understanding of the above-mentioned peculiar phenomena, we should reconsider the problem of how the size-dependent level structure of the exciton–radiation coupled system is determined in the non-LWA regime. By properly considering the interplay between their spatial structures in the microscopic nonlocal theory [23, 24], several peculiar aspects of the level structure in the non-LWA regime, such as a size-resonant enhancement of the radiative width and an interchange of the quantum states, have been predicted for a thin film and a spherical quantum dot [25–27]. Further, the mechanism of the above-mentioned size-resonant enhancement of the nonlinear response has been explained on the basis of such a level structure [28].

From the experimental viewpoint, some difficulties exist in the study of confined polaritons in the non-LWA regime. One of the challenges is a systematic preparation of qualified samples with different sizes, particularly for materials with a strong excitonic effect, such as II–VI and I–VII compounds. Among them, CuCl is a good prototype material for the investigation of excitons; the Z_3 exciton in CuCl has a large binding energy (197 meV) and exhibits a very strong radiative coupling. Recently, high-quality thin films of this material have been successfully fabricated by using the molecular beam epitaxy (MBE) technique associated with an electron beam radiation [29, 30] in which a high excitonic coherence is realized. An additional difficulty lies in the spectroscopic techniques. In the LWA regime, quantum states can be observed as spectral structures in the linear response spectra, such as transmittance and reflectance [7]. However, in the non-LWA regime, the assignment of quantum states is rather difficult because of the considerably large radiative correction and complicated interference effects. Further, the superposed waves of the scattering and incident light hide the structures of quantum states [15]. As one of the innovative methods to overcome such difficulties, non-degenerate two-photon scattering spectroscopy has been proposed, and it has succeeded in extracting the contributions from the excitonic scattering alone [29]; here, an anomalous mode structure exhibiting the interchange due to the large radiative correction has been revealed.

More recently, it has been theoretically demonstrated that resonant hyper-parametric scattering (RHPS) with the non-degenerate induced excitation of biexcitons is effective in revealing the polariton eigenmodes in nano-to-bulk thickness regions [31]. In non-degenerate two-photon scattering spectroscopy [29], one-exciton states are created with two photons, while in RHPS, biexcitons are resonantly created with two photons. In RHPS, the resonantly created biexcitons with no angular momentum collapse with the generation of polarization-correlated photon pairs conserving the angular momentum [32]. Itoh *et al* used this mechanism to determined the bulk polariton dispersion, where biexcitons are excited with two degenerate photons [33]. Triggered by the growing interest in quantum information technology, RHPS is now regarded as a process for generating entangled photon pairs [34, 35]. We expect that

this spectroscopy will be useful in observing the polariton level structure in the nano-to-bulk crossover regime. The weakness of the signal for a nanoscale sample is expected to be a problem. In order to overcome this problem, we propose a method using the non-degenerate induced excitation of biexcitons.

1.3. Purposes and organization of this article

The purposes of this article are to review the recent studies that have revealed the anomalous level structure of the exciton–radiation coupled system in a non-LWA regime, and to present the latest results from theoretical studies of the new method based on RHPS to observe polariton eigenmodes in the nano-to-bulk crossover regime.

In the first part, we review the theoretical prediction of the polariton level structure in the non-LWA regime and its experimental observation by non-degenerate two-photon scattering spectroscopy. We introduce the microscopic nonlocal theory [23] to calculate the polariton level structure by considering the long-range coherent coupling between the exciton and the radiation field, and discuss the calculated results. Subsequently, after presenting the nonlocal theory extended to analyse the results of non-degenerate two-photon scattering spectroscopy, we discuss the observed spectra and its corresponding analysis.

In the final part, we propose a new method based on RHPS to reveal the polariton level structure in the nano-to-bulk regime, and we give some calculations to reveal the potential of this method. Since the signal is due to the spontaneously emitted photons from the biexciton, the quantum mechanical treatment of the EM field is necessary to completely describe the motion of signal photons, and we have extended the semiclassical nonlocal theory to a full quantum one. Here, we will briefly explain this theory, and subsequently show the calculated spectra providing information of confined polariton modes in the nano-to-bulk crossover regime.

This article is organized as follows. In the next section, we explain the microscopic nonlocal response theory [23] and the model of the exciton with confined c.m. motion. In section 3, we present the calculated results of the eigenmodes of uncoupled excitons and those of a radiation–exciton coupled system (polaritons) confined in a thin film. For the latter result, the peculiar thickness dependence due to a very large radiative correction (shift and width) is discussed. In section 4, the theory to calculate the spectra by non-degenerate two-photon scattering spectroscopy is provided, and subsequently, we present the experimental results and their corresponding analyses. In section 5, we present a new quantum electrodynamics (QED) theory incorporating the excitonic nonlocality, and we give some calculations to discuss the potential of RHPS spectroscopy with non-degenerate induced excitation. The summary and future prospects are provided in section 6.

2. Theoretical framework and model of confined excitons

A particular feature of the optical response in the non-LWA regime is a large radiative correction arising from the self-consistent motion of radiation and matter. As a theoretical method to calculate the eigenmodes of confined polaritons exhibiting this effect, the microscopic nonlocal theory [23] is useful. In this section, we briefly explain this theory and the model of excitons having the c.m. motion as an origin of nonlocality.

2.1. Microscopic nonlocal theory for linear response

The principal task in the nonlocal theory is to solve the Maxwell equations for an electric field with an ω-Fourier component including the nonlocal susceptibility as follows:

$$\nabla \times \nabla \times \boldsymbol{E}(\boldsymbol{r}, \omega) - q^2 \epsilon_{\mathrm{b}}(\boldsymbol{r}) \boldsymbol{E}(\boldsymbol{r}, \omega) = 4\pi q^2 \boldsymbol{P}(\boldsymbol{r}, \omega), \tag{2}$$

where ω is the frequency, and $\boldsymbol{P}(\boldsymbol{r}, \omega)$ is expressed as

$$\boldsymbol{P}(\boldsymbol{r}, \omega) = \int \mathrm{d}\boldsymbol{r}' \, \chi(\boldsymbol{r}, \boldsymbol{r}'; \omega) \boldsymbol{E}(\boldsymbol{r}', \omega). \tag{3}$$

In these expressions, $\boldsymbol{E}(\boldsymbol{r}, \omega)$ is the electric field; $\boldsymbol{P}(\boldsymbol{r}, \omega)$, the induced polarization; $q = \omega/c$ with c the velocity of light; $\epsilon_{\mathrm{b}}(\boldsymbol{r})$, the position-dependent background dielectric constant; and $\chi(\boldsymbol{r}, \boldsymbol{r}'; \omega)$, the site-represented linear susceptibility. The resonance term is written as

$$\chi(\boldsymbol{r}, \boldsymbol{r}', \omega) = \sum_{\lambda} \frac{\boldsymbol{\rho}_{0\lambda}(\boldsymbol{r}) \boldsymbol{\rho}_{\lambda 0}(\boldsymbol{r}')}{E_\lambda - \hbar\omega - \mathrm{i}\Gamma}, \tag{4}$$

according to the Kubo formula, where λ is the index of quantum states of a matter system; E_λ, the eigenenergy of the state $|\lambda\rangle$; $\boldsymbol{\rho}_{\lambda 0}(\boldsymbol{r})$, the matrix of the dipole moment between the ground state and state $|\lambda\rangle$; and Γ, the phenomenologically introduced nonradiative damping constant. The solution of equation (2) is formally written as

$$\boldsymbol{E}(\boldsymbol{r}, \omega) = \boldsymbol{E}_{\mathrm{b}}(\boldsymbol{r}, \omega) + 4\pi q^2 \int \mathrm{d}\boldsymbol{r}' \, \bar{\boldsymbol{G}}(\boldsymbol{r}, \boldsymbol{r}', \omega) \cdot \boldsymbol{P}(\boldsymbol{r}', \omega), \tag{5}$$

where $\boldsymbol{E}_{\mathrm{b}}(\boldsymbol{r}, \omega)$ is the homogeneous solution, which is usually the incident field determined with Maxwell's boundary conditions, and $\bar{\boldsymbol{G}}(\boldsymbol{r}, \boldsymbol{r}', \omega)$ is the dyadic Green's function satisfying

$$\nabla \times \nabla \times \bar{\boldsymbol{G}}(\boldsymbol{r}, \boldsymbol{r}', \omega) - q^2 \epsilon_{\mathrm{b}}(\boldsymbol{r}) \bar{\boldsymbol{G}}(\boldsymbol{r}, \boldsymbol{r}', \omega) = \bar{\boldsymbol{I}} \delta(\boldsymbol{r} - \boldsymbol{r}'), \tag{6}$$

where $\bar{\boldsymbol{I}}$ is the unit dyad. In this stage, the formal solution (5) itself contains $\boldsymbol{E}(\boldsymbol{r}, \omega)$ by definition (3). The self-consistent equations (5) and (3) can be solved by using the separable form of susceptibility as in equation (4) with respect to the coordinates. Substituting equations (3) and (4) in (5) and defining the quantity

$$X_{\lambda 0} \equiv \frac{1}{E_\lambda - \hbar\omega - \mathrm{i}\Gamma} \int \mathrm{d}\boldsymbol{r} \, \boldsymbol{\rho}_{\lambda 0}(\boldsymbol{r}) \cdot \boldsymbol{E}(\boldsymbol{r}, \omega), \tag{7}$$

we obtain the following equation:

$$\boldsymbol{E}(\boldsymbol{r}, \omega) = \boldsymbol{E}_{\mathrm{b}}(\boldsymbol{r}, \omega) + 4\pi q^2 \sum_{\lambda} X_{\lambda 0} \int \mathrm{d}\boldsymbol{r}' \, \bar{\boldsymbol{G}}(\boldsymbol{r}, \boldsymbol{r}'; \omega) \cdot \boldsymbol{\rho}_{0\lambda}(\boldsymbol{r}'). \tag{8}$$

The volume integral of the inner product of $\boldsymbol{\rho}_{\lambda 0}(\boldsymbol{r})$ and $\boldsymbol{E}(\boldsymbol{r}, \omega)$ in this equation leads to linear simultaneous equations of $X_{\lambda 0}$ as follows:

$$(E_\lambda - \hbar\omega - \mathrm{i}\Gamma) X_{0\lambda} - \sum_{\nu} X_{0\nu} A_{\lambda\nu} = X_{0\lambda}^{(0)}, \tag{9}$$

where

$$A_{\lambda\lambda'} \equiv -4\pi q^2 \int \int \mathrm{d}\boldsymbol{r} \, \mathrm{d}\boldsymbol{r}' \, \boldsymbol{\rho}_{\lambda 0}(\boldsymbol{r}) \cdot \bar{\boldsymbol{G}}(\boldsymbol{r}, \boldsymbol{r}'; \omega) \cdot \boldsymbol{\rho}_{0\lambda'}(\boldsymbol{r}') \tag{10}$$

$$X_{\lambda 0}^{(0)} \equiv \int \mathrm{d}\boldsymbol{r} \, \boldsymbol{\rho}_{\lambda 0}(\boldsymbol{r}) \cdot \boldsymbol{E}_{\mathrm{b}}(\boldsymbol{r}, \omega). \tag{11}$$

It should be noted that $X_{\lambda 0}$ is the component arising from the λth excitonic state when we expand the induced polarization on the basis of excitonic wavefunctions. $A_{\lambda\lambda'}$ is the interaction between transition dipoles via the EM field, and $X_{\lambda 0}^{(0)}$ is the interaction between the transition dipole and an incident field. According to the definition of the Green's function $\bar{\boldsymbol{G}}(\boldsymbol{r}, \boldsymbol{r}', \omega)$, $A_{\lambda\lambda'}$ includes both retarded and instantaneous Coulomb interactions. Further, it should be noted

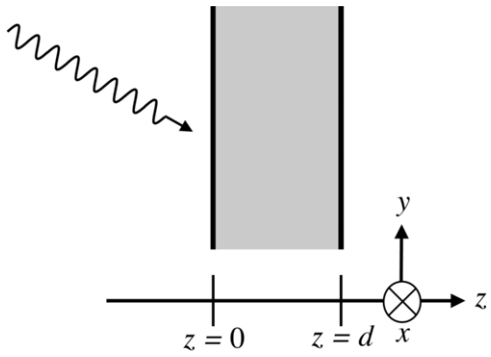

Figure 1. Geometry of the model for calculations.

that information on the spatial structure of the uncoupled radiation field reflecting the position-dependent background dielectric constant $\epsilon_{\rm b}(\boldsymbol{r})$ is included in $A_{\lambda\lambda'}$ through $\bar{\boldsymbol{G}}(\boldsymbol{r}, \boldsymbol{r}', \omega)$, and that of the matter wavefunction is included through $\boldsymbol{\rho}_{\lambda 0}(\boldsymbol{r})$. Thus, the interplay between the spatial structures of both of them appears through $A_{\lambda\lambda'}$. As for the specific expressions of the Green's function $\bar{\boldsymbol{G}}(\boldsymbol{r}, \boldsymbol{r}', \omega)$, the cases for the various types of geometries of the medium have been well studied so far [36]. Equation (9) can be expressed in matrix form as

$$\boldsymbol{S}\boldsymbol{X} = \boldsymbol{X}^{(0)}. \tag{12}$$

If we solve this equation as $\boldsymbol{X} = \boldsymbol{S}^{-1}\boldsymbol{X}^{(0)}$, the total field at arbitrary positions can be obtained as

$$\boldsymbol{E}(\boldsymbol{r}, \omega) = \boldsymbol{E}_{\rm b}(\boldsymbol{r}, \omega) + \sum_{\lambda} X_{\lambda} \boldsymbol{B}_{\lambda}(\boldsymbol{r}, \omega), \tag{13}$$

where

$$\boldsymbol{B}_{\lambda}(\boldsymbol{r}) \equiv 4\pi q^2 \int {\rm d}\boldsymbol{r}'\, \bar{\boldsymbol{G}}(\boldsymbol{r}, \boldsymbol{r}'; \omega) \cdot \boldsymbol{\rho}_{0\lambda}(\boldsymbol{r}'). \tag{14}$$

Further, the roots of $\det \mathbf{S} = 0$ provide the complex eigenmodes (Ω_n) of the coupled system, whose real parts $\{{\rm Re}[\Omega_n]\}$ include the radiative shift, and the imaginary parts $\{{\rm Im}[\Omega_n]\}$ correspond to the radiative decay rate.

2.2. Model of confined excitons

As a model system, we consider a thin film where the c.m. motion of the excitons is confined in the direction of the film thickness along the z-axis, as illustrated in figure 1. The film has a thickness d and is periodic in the xy-plane. The excitonic Bohr radius is assumed to be much smaller than the film thickness and we consider the relative motion of the excitons as that in bulk and consider only the 1s state. The surfaces act as infinite potential walls for the c.m. motion; hence, the distortions of the c.m. wavefunctions near the surfaces are neglected. Assuming that the wavenumber K_n along the film thickness is quantized as

$$K_n = n\pi/d \tag{15}$$

with a positive integer n and a wavevector $\boldsymbol{K}_{\parallel}$ parallel to the film surface, we write the kinetic energy part $\tilde{E}_n$, and its wavefunction ψ can be given as

$$\tilde{E}_{n,K_{\parallel}} = \frac{\hbar^2}{2M}(K_n^2 + K_{\parallel}^2), \tag{16}$$

$$\psi_{n,\boldsymbol{K}_{\parallel}}(\boldsymbol{r}) = \frac{1}{\sqrt{S}} {\rm e}^{{\rm i}\boldsymbol{K}_{\parallel}\cdot\boldsymbol{r}_{\parallel}} \sqrt{\frac{2}{d}} \sin K_n z, \tag{17}$$

where M is the translational mass of an exciton; $\boldsymbol{r}$, the position of c.m., whose parallel component is $\boldsymbol{r}_\parallel$; and S, an area along the film surface. Namely, each quantum state is labelled by n, $\boldsymbol{K}_\parallel$, and polarization direction $\xi(= x, y, z)$ as

$$|\lambda\rangle = |n, \boldsymbol{K}_\parallel, \xi\rangle. \tag{18}$$

Since $\boldsymbol{K}_\parallel$ is the good quantum number of this system, we can consider the subspace with fixed $\boldsymbol{K}_\parallel$. Thus, the wavefunction $\Psi_n(\boldsymbol{r})$ of the excitons and the total energy E_n are described as

$$\Psi_{n\boldsymbol{K}_\parallel}(\boldsymbol{r}) = \phi_{1\mathrm{s}}\psi_{n,\boldsymbol{K}_\parallel}(\boldsymbol{r}),$$
$$E_{n\boldsymbol{K}_\parallel} = \hbar\omega_{\mathrm{T}} + \tilde{E}_{n,\boldsymbol{K}_\parallel},$$

where $\phi_{1\mathrm{s}}$ is the wavefunction of 1s relative motion, which is taken at zero electron–hole separation, and $\hbar\omega_{\mathrm{T}}$ is the energy of the bulk transverse exciton. The matrix element of the transition dipole density $\boldsymbol{\rho}_{\lambda 0}(\boldsymbol{r})$ of this model is

$$\boldsymbol{\rho}_{\lambda 0}(\boldsymbol{r}) = \mu\hat{\boldsymbol{\xi}}\psi_{n\boldsymbol{K}_\parallel}(\boldsymbol{r}), \tag{19}$$

where $\hat{\boldsymbol{\xi}}$ is the unit vector along the ξ-axis, and μ can be described as

$$\mu^2 = \frac{\epsilon_{\mathrm{b}}\Delta_{\mathrm{LT}}}{4\pi}, \tag{20}$$

where ϵ_{b} is the background dielectric constant of the medium and Δ_{LT} is the split energy between the transverse excitonic energy $\hbar\omega_{\mathrm{T}}$ and the longitudinal excitonic energy $\hbar\omega_{\mathrm{L}}$ in the bulk.

3. Exciton–radiation coupled modes in a thin film

In this section, we present the calculated level structures. First, we show the eigenmodes of uncoupled excitons, where we neglect the retarded interaction by considering only the longitudinal interaction in $A_{\lambda\lambda'}$. The longitudinal interaction includes an exchange interaction between excitons, and an interaction between the exciton and image charges due to the surfaces that arises from the background dielectric constant. Further, we show the level structure of the exciton–radiation coupled system (polaritons) considering the retarded interaction. We particularly observe a drastic change in the level structure due to the extremely large radiative correction.

3.1. Level structure of uncoupled excitons

In the following calculations, we use the material parameters of the Z_3 exciton in CuCl, which is a typical Wannier-type exciton with a small Bohr radius (6–7 Å) and large binding energy (197 meV), namely,

Background dielectric constant: $\epsilon_{\mathrm{b}} = 5.59$ [37]. (21)

Total mass: $M = 2.3\, m_0$ (m_0: rest mass of the free electron) [37]. (22)

LT-splitting energy: $\Delta_{\mathrm{LT}} = 5.7$ meV [38]. (23)

Energy of the transverse exciton in the bulk: $\hbar\omega_{\mathrm{T}} = 3.2022$ eV [38]. (24)

Lattice constant: $a = 5.4$ Å. (25)

Figure 2 shows the eigenenergies of excitons as functions of the film thickness. We give the value of $K_\parallel$ through θ with the definition $K_\parallel = (\omega_T/c)\sin\theta$. For $K_\parallel = 0$, the modes of transverse excitons doubly degenerate due to the degrees of freedom of the polarization and those of longitudinal excitons. They strongly reflect the size quantization effect when d is small,

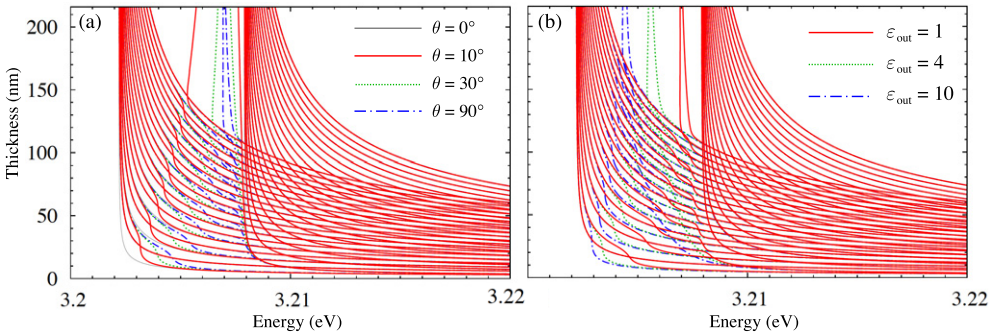

Figure 2. Eigenmodes in the absence of retarded interaction between the induced polarizations. (a) Dependence on $K_\parallel$. $K_\parallel$ is given as $K_\parallel = (\omega_T/c)\sin\theta$. (b) Dependence on ϵ_{out}.

while both kinds of modes approach the energy of the transverse and longitudinal excitons, respectively, with an increase in the thickness. In the case of finite $K_\parallel$, pure transverse modes, which we call TE-modes, and transverse and longitudinal mixed modes, which we call TM-modes, arise. In the absence of the retarded interaction, the TE-modes do not interact with each other. In the LT-splitting region, two surface modes can be seen, and they are mixed with the TM-modes. For a sufficiently thick region, these two modes degenerate, while this degeneration is removed in the thinner region because of the interaction between the two modes of the respective surfaces. Since the larger $K_\parallel$ leads to the smaller attenuation constant of the evanescent wave of the surface modes, the energy splitting is smaller for a larger $K_\parallel$, as shown in figure 2(a). The dependence of the surface mode energies on the dielectric constant outside the media is shown in figure 2(b). This dependence is attributed to the dependence of the image potential at the surfaces on the difference between the background dielectric constant of the medium and that outside the medium.

3.2. Level structure of an exciton–radiation coupled system

If retarded interaction is considered, the level structure is drastically changed. Figure 3 shows the results of the calculations in the presence of retarded interaction. In general, coupled modes have both real and imaginary parts. The latter quantity corresponds to the radiative width explained in section 2. In the case of $K_\parallel = 0$, the longitudinal modes do not couple with the radiation, so no shift can be observed (no figure). On the other hand, the two kinds of (doubly degenerate) transverse modes exhibit a large enhancement in both the shift and width for each mode at a certain thickness. One of the characteristic features of the coupled modes is such a remarkable thickness dependence of the radiative collection, which can be seen in the non-LWA regime. The change in the mutual relationship between the spatial structures of the radiation and excitonic wavefunctions drastically varies the interaction strength between them, depending on the film thickness. The interchange in the quantum states and size-resonant behaviour of both the real and imaginary parts are particularly interesting phenomena. Hereafter, the number n denotes the polariton mode whose original uncoupled exciton state is $|n, \boldsymbol{K}_\parallel, \xi\rangle$.

On comparing the levels of the uncoupled excitons with the coupled modes in figure 3(a), we can see that the radiative shift of the lowest state is always positive, while all the other states have negative shift when the thickness is small. For the lowest state, the eigenenergy increases with the thickness and finally approaches the energy of a bulk longitudinal exciton ($\hbar\omega_{\text{L}}$). For the latter states, the eigenenergies decrease with the thickness at the initial stage; however, they

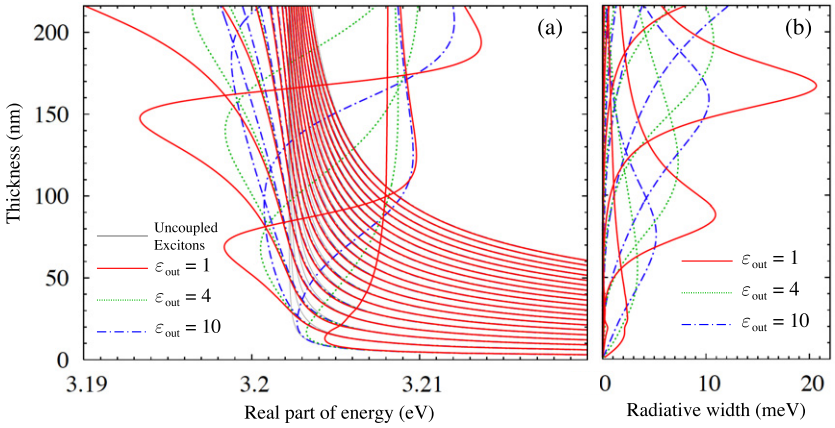

Figure 3. Thickness dependence of the complex eigenmodes in the presence of retarded interaction between the induced polarizations. (a) Real parts (eigenenergies including the radiative shift). (b) Imaginary parts (radiative width).

then begin to increase and jump to the higher energy side at certain thickness regions for the respective modes and also approach $\hbar\omega_{\mathrm{L}}$. In other words, their lower polariton nature changes to an upper polariton one at the thickness where a particular relationship condition between the spatial structures of the radiation and excitonic wavefunction is satisfied. This behaviour leads to the interchange of quantum states. Such a property is comprehended by enquiring into the dependence of the exciton energy on the wavenumber $(n\pi/d)$. As shown in figure 3(a), every state jumps from the lower to the upper branch. We note that the jump occurs when $2d/n$ is of the same order as the corresponding radiation wavelength. Since the interaction length of an exciton and radiation determines the coupling strength, the jump height is related to the film thickness d. In the infinity limit of the film thickness, these quantum states jump from 0 to infinity. This behaviour agrees with upper polariton branch (UPB) or lower polariton branch (LPB) of the bulk polariton.

The imaginary parts of the respective modes, i.e., the radiative widths, are shown in figure 3(b). The size-linear increase is observed for $n = 1$ at the initial stage of the increase in thickness. This is the previously discussed size-linear enhancement due to the same behaviour of the excitonic oscillator strength [3, 4]. However, this enhancement is almost immediately saturated, and starts to decrease. Then, the width of the $n = 2$ exciton increases and takes a maximum value. The interaction strength becomes maximum at this time. Subsequently, it begins to decrease. It should be noted that the radiative width of each mode acquires a maximum value at the same time as the jump of the real part. As shown in this figure, the thickness dependence of the radiative width in the non-LWA regime is not monotonic. This indicates that there is a wide degree of freedom to control the radiation–matter coupling strength in the non-LWA regime.

4. Observation of level structure in the non-LWA regime

As explained in the previous section, the thickness dependence of the eigenmodes of confined polaritons is significantly different from that of uncoupled excitons in the non-LWA regime. This situation leads to the anomalous thickness dependence of various types of optical effects, such as nonlinear response, radiative decay, etc, which cannot be determined only from the

properties of uncoupled excitons. However, it is not easy to experimentally verify this level structure with conventional one-photon spectroscopy. To extract the contributions from the pure scattered signals due to the coupled eigenstates, two-photon spectroscopy is useful. In this method, the energy of the incident light is distant from that of the exciton, and interference effects can be avoided. In this section, we present a new technique—'non-degenerate two-photon excitation scattering' [29]—along with the corresponding theoretical method. First, we introduce a theoretical method to analyse the results by two-photon excitation scattering, which is an extension of the microscopic nonlocal theory. Subsequently, the experimental results and their analysis are presented.

4.1. Nonlocal theory of two-photon excitation scattering

In this subsection, we extend the above-mentioned microscopic nonlocal theory to calculate the total frequency generation, which is described as a second-order nonlinear process. The first- and second-order induced polarization can be written using the Fourier components $\boldsymbol{E}(\boldsymbol{r}, \omega)$ of the total EM field with frequency ω, as

$$\boldsymbol{P}^{(1)}(\boldsymbol{r}, \omega) = \int \mathrm{d}\boldsymbol{r}'\, \bar{\boldsymbol{\chi}}^{(1)}(\boldsymbol{r}, \boldsymbol{r}'; \omega) \cdot \boldsymbol{E}(\boldsymbol{r}', \omega) \tag{26}$$

$$\boldsymbol{P}^{(2)}(\boldsymbol{r}, \omega = \omega_1 + \omega_2) = \int \mathrm{d}\boldsymbol{r}' \int \mathrm{d}\boldsymbol{r}''\, \bar{\boldsymbol{\chi}}^{(2)}(\boldsymbol{r}, \boldsymbol{r}', \boldsymbol{r}''; \omega_1, \omega_2) \cdot \boldsymbol{E}(\boldsymbol{r}', \omega_1) \cdot \boldsymbol{E}(\boldsymbol{r}'', \omega_2). \tag{27}$$

The Maxwell equation that these polarizations should satisfy is

$$\nabla \times \nabla \times \boldsymbol{E}(\boldsymbol{r}, \omega) - q^2 \epsilon_{\mathrm{b}}(\boldsymbol{r}) \boldsymbol{E}(\boldsymbol{r}, \tilde{\omega}) = 4\pi q^2 \left[\boldsymbol{P}^{(1)}(\boldsymbol{r}, \omega) + \boldsymbol{P}^{(2)}(\boldsymbol{r}, \omega = \omega_1 + \omega_2) \right], \tag{28}$$

where $q = \omega/c$ is the wavenumber of light with the frequency ω in vacuum and $\epsilon_{\mathrm{b}}(\boldsymbol{r})$ is the background dielectric constant including information on the spatial structure of the medium. $\epsilon_{\mathrm{b}}(\boldsymbol{r})$ is assumed to be constant in and outside the medium.

We consider the two-photon excitation scattering as a second nonlinear process. We assume that the two kinds of incident light with $\boldsymbol{E}(\omega_1)$ and $\boldsymbol{E}(\omega_2)$, whose frequencies are off-resonance with the excitons, are determined within the linear response. Further, it is considered that the scattered signal light with $\boldsymbol{E}(\omega)$ does not contribute to the two-photon absorption process. Under these assumptions, we rewrite the total electric field as

$$\boldsymbol{E}(\boldsymbol{r}, t) = \boldsymbol{E}(\boldsymbol{r}, \omega_1) \mathrm{e}^{\mathrm{i}\omega_1 t} + \boldsymbol{E}(\boldsymbol{r}, \omega_2) \mathrm{e}^{\mathrm{i}\omega_2 t} + \boldsymbol{E}(\boldsymbol{r}, \omega_s) \mathrm{e}^{\mathrm{i}\omega_s t}. \tag{29}$$

From this expression, the induced polarization is described as

$$\boldsymbol{P}^{(1)}(\boldsymbol{r}, \omega) = \int \mathrm{d}\boldsymbol{r}'\, \chi^{(1)}(\boldsymbol{r}, \boldsymbol{r}'; \omega) \boldsymbol{E}(\boldsymbol{r}', \omega), \tag{30}$$

$$\begin{aligned} \boldsymbol{P}^{(2)}(\boldsymbol{r}, \omega = \omega_1 + \omega_2) = {} & \int \mathrm{d}\boldsymbol{r}_1 \int \mathrm{d}\boldsymbol{r}_2\, \bar{\boldsymbol{\chi}}^{(2)}(\boldsymbol{r}, \boldsymbol{r}_1, \boldsymbol{r}_2; \omega_1, \omega_2) \cdot \boldsymbol{E}(\boldsymbol{r}_1, \omega_1) \cdot \boldsymbol{E}(\boldsymbol{r}_2, \omega_2) \\ & + \int \mathrm{d}\boldsymbol{r}_1 \int \mathrm{d}\boldsymbol{r}_2\, \bar{\boldsymbol{\chi}}^{(2)}(\boldsymbol{r}, \boldsymbol{r}_1, \boldsymbol{r}_2; \omega_2, \omega_1) \cdot \boldsymbol{E}(\boldsymbol{r}_1, \omega_2) \cdot \boldsymbol{E}(\boldsymbol{r}_2, \omega_1). \end{aligned} \tag{31}$$

The first and second terms on the right-hand side of equation (31) represent the transition from the ground state to the intermediate excited state by light with frequencies ω_2 and ω_1, respectively. Thus, the Maxwell equations for the electric fields with frequencies ω and ω_j $(j = 1, 2)$ are

$$\nabla \times \nabla \times \boldsymbol{E}(\boldsymbol{r}, \omega) - q^2 \epsilon_{\mathrm{b}}(\boldsymbol{r}) \boldsymbol{E}(\boldsymbol{r}, \omega) = 4\pi q^2 [\boldsymbol{P}^{(1)}(\boldsymbol{r}, \omega) + \boldsymbol{P}^{(2)}(\boldsymbol{r}, \omega = \omega_1 + \omega_2)], \tag{32}$$

$$\nabla \times \nabla \times \boldsymbol{E}_j(\boldsymbol{r}, \omega_j) - q_j^2 \epsilon_{\mathrm{b}}(\boldsymbol{r}) \boldsymbol{E}_j(\boldsymbol{r}, \omega_j) = \boldsymbol{0} \qquad (j = 1, 2). \tag{33}$$

Since there is no incident field with the frequency ω, the solution of equation (32) is written as

$$\boldsymbol{E}(\boldsymbol{r},\omega) = 4\pi q^2 \int \mathrm{d}\boldsymbol{r}'\, \bar{\boldsymbol{G}}(\boldsymbol{r},\boldsymbol{r}',\omega)\cdot[\boldsymbol{P}^{(1)}(\boldsymbol{r}',\omega)+\boldsymbol{P}^{(2)}(\boldsymbol{r}',\omega=\omega_1+\omega_2)], \tag{34}$$

where the definition of dyadic Green's function $\bar{\boldsymbol{G}}(\boldsymbol{r},\boldsymbol{r}',\omega)$ is the same as equation (6). Defining the susceptibilities of resonant induced polarizations as

$$\bar{\boldsymbol{\chi}}^{(1)}(\boldsymbol{r},\boldsymbol{r}';\omega) = \sum_{\lambda} \frac{\boldsymbol{\rho}_{0\lambda}(\boldsymbol{r})\boldsymbol{\rho}_{\lambda 0}(\boldsymbol{r}')}{E_\lambda - \hbar\omega - \mathrm{i}\Gamma}, \tag{35}$$

$$\bar{\boldsymbol{\chi}}^{(2)}(\boldsymbol{r},\boldsymbol{r}_1,\boldsymbol{r}_2;\omega_1,\omega_2) = \sum_{\lambda_1}\sum_{\lambda_2} \frac{\boldsymbol{\rho}_{0\lambda_2}(\boldsymbol{r})\boldsymbol{\rho}_{\lambda_1 0}(\boldsymbol{r}_2)\boldsymbol{\rho}_{\lambda_2\lambda_1}(\boldsymbol{r}_1)}{(E_{\lambda_1}-\hbar\omega_2-\mathrm{i}\Gamma)(E_{\lambda_2}-\hbar\omega-\mathrm{i}\Gamma)}, \tag{36}$$

$$\bar{\boldsymbol{\chi}}^{(2)}(\boldsymbol{r},\boldsymbol{r}_1,\boldsymbol{r}_2;\omega_2,\omega_1) = \sum_{\lambda_1}\sum_{\lambda_2} \frac{\boldsymbol{\rho}_{0\lambda_2}(\boldsymbol{r})\boldsymbol{\rho}_{\lambda_1 0}(\boldsymbol{r}_2)\boldsymbol{\rho}_{\lambda_2\lambda_1}(\boldsymbol{r}_1)}{(E_{\lambda_1}-\hbar\omega_1-\mathrm{i}\Gamma)(E_{\lambda_2}-\hbar\omega-\mathrm{i}\Gamma)}, \tag{37}$$

and substituting equations (30), (31), and (35)–(37) in (34), we obtain the expression

$$\begin{aligned}\boldsymbol{E}(\boldsymbol{r},\omega) = 4\pi q^2 \int \mathrm{d}\boldsymbol{r}'\, \bar{\boldsymbol{G}}(\boldsymbol{r},\boldsymbol{r}';\omega)\Bigg\{ &\int \mathrm{d}\boldsymbol{r}' \sum_{\lambda} \frac{\boldsymbol{\rho}_{0\lambda}(\boldsymbol{r})\boldsymbol{\rho}_{\lambda 0}(\boldsymbol{r}')}{E_\lambda-\hbar\omega-\mathrm{i}\Gamma}\cdot\boldsymbol{E}(\boldsymbol{r}',\omega)\\ &+\int \mathrm{d}\boldsymbol{r}_1 \int \mathrm{d}\boldsymbol{r}_2 \sum_{\lambda_1}\sum_{\lambda_2} \frac{\boldsymbol{\rho}_{0\lambda_2}(\boldsymbol{r})\boldsymbol{\rho}_{\lambda_1 0}(\boldsymbol{r}_2)\boldsymbol{\rho}_{\lambda_2\lambda_1}(\boldsymbol{r}_1)}{(E_{\lambda_1}-\hbar\omega_2-\mathrm{i}\Gamma)(E_{\lambda_2}-\hbar\omega-\mathrm{i}\Gamma)}\cdot\boldsymbol{E}_1(\boldsymbol{r}_1,\omega_1)\\ &\cdot\boldsymbol{E}_2(\boldsymbol{r}_2,\omega_2)+\int \mathrm{d}\boldsymbol{r}_1 \int \mathrm{d}\boldsymbol{r}_2 \sum_{\lambda_1}\sum_{\lambda_2} \frac{\boldsymbol{\rho}_{0\lambda_2}(\boldsymbol{r})\boldsymbol{\rho}_{\lambda_1 0}(\boldsymbol{r}_2)\boldsymbol{\rho}_{\lambda_2\lambda_1}(\boldsymbol{r}_1)}{(E_{\lambda_1}-\hbar\omega_1-\mathrm{i}\Gamma)(E_{\lambda_2}-\hbar\omega-\mathrm{i}\Gamma)}\\ &\cdot\boldsymbol{E}_2(\boldsymbol{r}_1,\omega_2)\cdot\boldsymbol{E}_1(\boldsymbol{r}_2,\omega_1)\Bigg\},\end{aligned} \tag{38}$$

where $\boldsymbol{\rho}_{\lambda' 0}\boldsymbol{\rho}_{\lambda\lambda'}\cdot\boldsymbol{E}_j\cdot\boldsymbol{E}_i$ means $(\boldsymbol{\rho}_{\lambda\lambda'}\cdot\boldsymbol{E}_j)(\boldsymbol{\rho}_{\lambda' 0}\cdot\boldsymbol{E}_i)$. Multiplying both sides of this equation by $\rho_{\lambda 0}(\boldsymbol{r})$, and integrating over $\boldsymbol{r}$, we obtain the equation

$$\begin{aligned}\int \mathrm{d}\boldsymbol{r}\,\boldsymbol{\rho}_{\lambda 0}(\boldsymbol{r})\cdot\boldsymbol{E}(\boldsymbol{r},\omega) = 4\pi q^2 \sum_{\lambda'}\int \mathrm{d}\boldsymbol{r}\int \mathrm{d}\boldsymbol{r}'\,\boldsymbol{\rho}_{\lambda 0}(\boldsymbol{r})\cdot\bar{\boldsymbol{G}}(\boldsymbol{r},\boldsymbol{r}';\omega)\cdot\boldsymbol{\rho}_{0\lambda'}(\boldsymbol{r}')\\ \times\Bigg\{\int \mathrm{d}\boldsymbol{r}''\,\frac{\boldsymbol{\rho}_{\lambda' 0}(\boldsymbol{r}'')\cdot\boldsymbol{E}(\boldsymbol{r}'',\omega)}{E_{\lambda'}-\hbar\omega-\mathrm{i}\Gamma}\\ +\sum_{\lambda''}\Bigg[\int \mathrm{d}\boldsymbol{r}''\int \mathrm{d}\boldsymbol{r}'''\,\frac{\boldsymbol{\rho}_{\lambda'' 0}(\boldsymbol{r}'')\boldsymbol{\rho}_{\lambda'\lambda''}(\boldsymbol{r}''')\cdot\boldsymbol{E}_1(\boldsymbol{r}''',\omega_1)\cdot\boldsymbol{E}_2(\boldsymbol{r}'',\omega_2)}{(E_{\lambda'}-\hbar\omega-\mathrm{i}\Gamma)(E_{\lambda''}-\hbar\omega_2-\mathrm{i}\Gamma)}\\ +\int \mathrm{d}\boldsymbol{r}''\int \mathrm{d}\boldsymbol{r}'''\,\frac{\boldsymbol{\rho}_{\lambda'' 0}(\boldsymbol{r}'')\boldsymbol{\rho}_{\lambda'\lambda''}(\boldsymbol{r}''')\cdot\boldsymbol{E}_2(\boldsymbol{r}''',\omega_2)\cdot\boldsymbol{E}_1(\boldsymbol{r}'',\omega_1)}{(E_{\lambda'}-\hbar\omega-\mathrm{i}\Gamma)(E_{\lambda''}-\hbar\omega_1-\mathrm{i}\Gamma)}\Bigg]\Bigg\}.\end{aligned} \tag{39}$$

Defining the quantities

$$X_\lambda \equiv \frac{1}{E_\lambda-\hbar\omega-\mathrm{i}\Gamma}\int \mathrm{d}\boldsymbol{r}\,\boldsymbol{\rho}_{\lambda 0}(\boldsymbol{r})\cdot\boldsymbol{E}(\boldsymbol{r},\omega), \tag{40}$$

$$A_{\lambda\lambda'} \equiv -4\pi q^2 \int \mathrm{d}\boldsymbol{r}\int \mathrm{d}\boldsymbol{r}'\,\boldsymbol{\rho}_{\lambda 0}(\boldsymbol{r})\cdot\bar{\boldsymbol{G}}(\boldsymbol{r},\boldsymbol{r}';\omega)\cdot\boldsymbol{\rho}_{0\lambda'}(\boldsymbol{r}'), \tag{41}$$

$$X^{(2)}_\lambda \equiv \frac{1}{E_\lambda-\hbar\omega-\mathrm{i}\Gamma}\sum_{\lambda'}\tilde{X}^{(2)}_{\lambda\lambda'}, \tag{42}$$

$$\begin{aligned}\tilde{X}^{(2)}_{\lambda\lambda'} \equiv &\frac{1}{E_{\lambda'}-\hbar\omega_2-\mathrm{i}\Gamma}\int \mathrm{d}\boldsymbol{r}\int \mathrm{d}\boldsymbol{r}'\,\boldsymbol{\rho}_{\lambda\lambda'}(\boldsymbol{r}')\boldsymbol{\rho}_{\lambda' 0}(\boldsymbol{r})\cdot\boldsymbol{E}_1(\boldsymbol{r}',\omega_1)\cdot\boldsymbol{E}_2(\boldsymbol{r},\omega_2)\\ &+\frac{1}{E_{\lambda'}-\hbar\omega_1-\mathrm{i}\Gamma}\int \mathrm{d}\boldsymbol{r}\int \mathrm{d}\boldsymbol{r}'\,\boldsymbol{\rho}_{\lambda\lambda'}(\boldsymbol{r}')\boldsymbol{\rho}_{\lambda' 0}(\boldsymbol{r})\cdot\boldsymbol{E}_2(\boldsymbol{r}',\omega_2)\cdot\boldsymbol{E}_1(\boldsymbol{r},\omega_1),\end{aligned} \tag{43}$$

we can rewrite equation (39) as

$$(E_\lambda - \hbar\omega - \mathrm{i}\Gamma)X_\lambda + \sum_{\lambda'} A_{\lambda\lambda'}[X_{\lambda'} + X^{(2)}_{\lambda'}] = 0. \tag{44}$$

This equation can be expressed in matrix form as

$$\begin{pmatrix} E_1 + A_{11} - \mathrm{i}\Gamma - \hbar\omega & A_{12} & \cdots \\ A_{21} & E_2 + A_{22} - \mathrm{i}\Gamma - \hbar\omega & \cdots \\ \vdots & \vdots & \ddots \end{pmatrix} \begin{pmatrix} X_1 \\ X_2 \\ \vdots \end{pmatrix}$$

$$= -\begin{pmatrix} A_{11} & A_{12} & \cdots \\ A_{21} & A_{22} & \cdots \\ \vdots & \vdots & \ddots \end{pmatrix} \begin{pmatrix} X^{(2)}_1 \\ X^{(2)}_2 \\ \vdots \end{pmatrix} \tag{45}$$

$$\Longleftrightarrow \boldsymbol{S}\boldsymbol{X} = -\boldsymbol{A}\boldsymbol{X}^{(2)}. \tag{46}$$

Since the $X^{(2)}_\lambda$ are known values, if $E_1(\boldsymbol{r}, \omega_1)$ and $E_2(\boldsymbol{r}, \omega_2)$ are determined by independent Maxwell equations, this equation system can be used to determine $\{X_\lambda\}$. Obtaining the unknown vector $\boldsymbol{X}$ as

$$\boldsymbol{X} = -\boldsymbol{S}^{-1}\boldsymbol{A}\boldsymbol{X}^{(2)}, \tag{47}$$

the response field $\boldsymbol{E}(\boldsymbol{r}, \omega)$ is determined from equation (38) as

$$\boldsymbol{E}(\boldsymbol{r}, \omega) = \sum_\lambda [X_\lambda + X^{(2)}_\lambda]\boldsymbol{B}_\lambda(\boldsymbol{r}, \omega), \tag{48}$$

where $\boldsymbol{B}_\lambda(\boldsymbol{r}, \omega)$ is

$$\boldsymbol{B}_\lambda(\boldsymbol{r}, \omega) \equiv 4\pi q^2 \int \mathrm{d}\boldsymbol{r}'\, \bar{\boldsymbol{G}}(\boldsymbol{r}, \boldsymbol{r}'; \omega) \cdot \boldsymbol{\rho}_{0\lambda}(\boldsymbol{r}'). \tag{49}$$

In equations (36) and (37), $\boldsymbol{\rho}_{\lambda\lambda'}(\boldsymbol{r})$ indicates the transition matrix element between one-exciton states. Namely,

$$\boldsymbol{\rho}_{\lambda\lambda'}(\boldsymbol{r}) = \psi^*_\lambda(\boldsymbol{r})\psi_{\lambda'}(\boldsymbol{r})(\boldsymbol{d}_{\mathrm{cc}} + \boldsymbol{d}_{\mathrm{vv}}), \tag{50}$$

where $\boldsymbol{d}_{\mathrm{cc}}$ and $\boldsymbol{d}_{\mathrm{vv}}$ are the dipole matrix elements between the conduction states and valence states, respectively. In the case of CuCl, these matrix elements are finite because of the crystal symmetry, although they are small. The magnitude of $\bar{\boldsymbol{\chi}}^{(2)}$ is proportional to $|\boldsymbol{d}_{\mathrm{cc}} + \boldsymbol{d}_{\mathrm{vv}}|$. In the following calculations, we take note of the combination of incident direction and polarization that yields a finite value of $\bar{\boldsymbol{\chi}}^{(2)}$ from the viewpoint of group theory; however, we do not estimate its absolute value. Although the absolute value of the signal intensity depends on this value, the spectral shape, which is our concern, does not depend on it.

In [29], a different type of calculation method with a more intuitive description is presented for the analysis of the experimental data. Although this method seems to be different from the present theory, it can be verified that these two methods provide the same results.

4.2. Experimental results and analyses

In the experiment [29], a CuCl single crystal was grown using the vapour growth technique. The thickness of the CuCl films was estimated from the growth rate and measurement using atomic force microscopy (AFM). The sample was simultaneously excited by a 1064 nm line, the fundamental light of an Nd:YAG laser, and the light of a dye laser excited by the 532 nm line of the second harmonic of the same Nd:YAG laser. A dye laser of rhodamine 610 in ethanol was scanned from 600 to 612 nm. When the sum energy of the photons from the two lasers resonates with the Z_3 (1s) exciton energy of CuCl, excitons will be generated. Photons

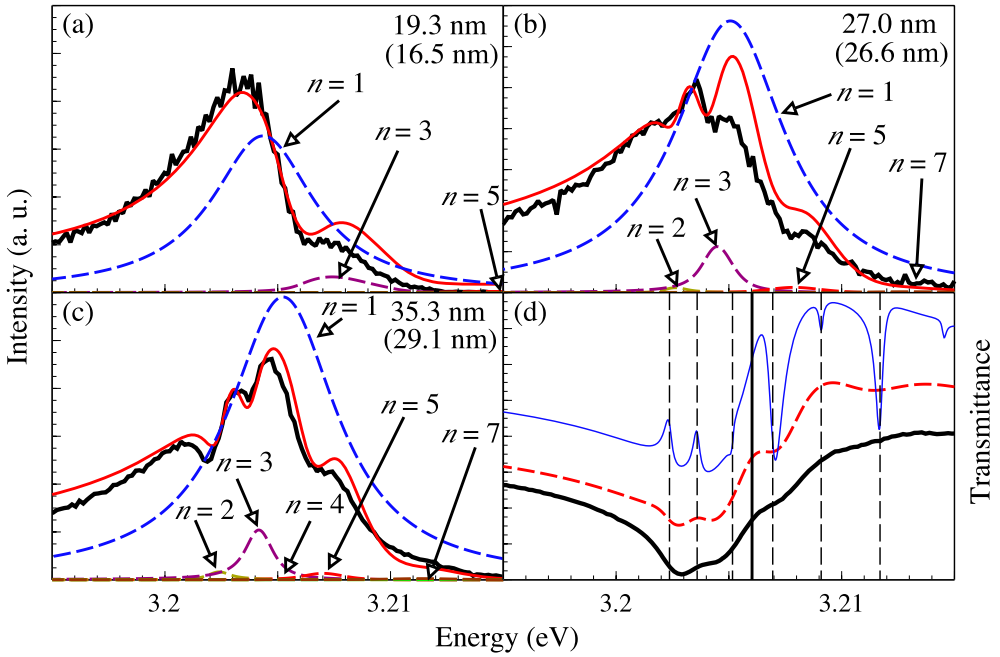

Figure 4. (a)–(c) Measured (thick solid line) and calculated (normal solid line) two-photon scattering spectra of CuCl films with different thicknesses. The calculated components of individual quantum states are shown by dotted curves. (d) Thin solid and broken lines are the calculated transmission spectra for a thickness of 29.1 nm using nonradiative damping with energies of 0.1 and 0.4 meV, respectively. The thick solid line shows the measured transmission spectrum for 35.3 nm. Broken vertical lines indicate the polariton level including radiative shift from $n = 2$ to 7 in order from the lowest energy. The solid vertical line indicates the polariton level of $n = 1$. From this figure, we observe that it is impossible to identify the position of $n = 1$ in the transmission spectrum.

with the same amount of energy will be generated through the radiative decay of excitons and are scattered from the sample. The measurement was performed with a backward-scattering configuration. The temperature of the sample was 10 K. For comparison, the transmission spectra were also measured under normal incidence using a tungsten lamp.

Figure 4 shows the measured results for films having thickness from 19.3 to 35.3 nm (thick solid lines). In the thinner case, the peak positions are very similar to the dip positions of linear transmittance (no figure). This means that we can extract information on the eigenmodes of polaritons from the transmittance of rather thin films [7]. However, in the thicker films, the structures in the transmittance do not necessarily coincide with those in the two-photon scattering spectra. This can be seen by comparing the spectrum in figure 4(c) and the corresponding transmittance spectrum in figure 4(d). In the case of thicker films, a complicated interference effect obscures information on the eigenstates of polaritons in the transmittance spectrum. The manner in which the two-photon scattering spectra provide this information can be understood by examining the following analysis. In figures 4(a)–(c), we show the comparisons between the experimental and the calculated spectra. In these calculations, we used the following parameters: refractive index $n = 1.97$ for 610 nm and $n = 1.92$ [39] for 1064 nm, and nonradiative damping constant 0.4 meV. The other excitonic parameters are the same as those in figure 2. The calculation was broadened by assuming a Gaussian fluctuation of 5% in film thickness. Although there is a mismatch in the film thickness, which may result

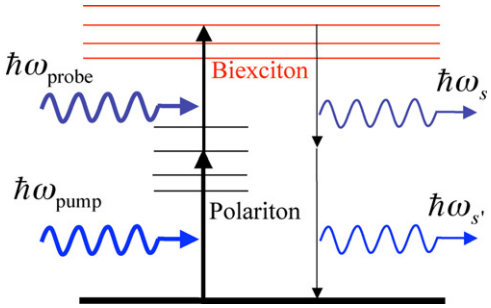

Figure 5. Schematic diagram of RHPS by induced excitation of a biexciton.

from errors in the measurement of the growth rate, we can see that agreements between the measured and calculated spectra are excellent.

The dotted curves in figures 4(a)–(c) show the components of every quantum state. The spectrum of a 19.3 nm thick film is constructed only from odd states $n = 1, 3, 5, \ldots$. This shows that the LWA is valid in this thickness. On the other hand, for a film with a thickness of 35.3 nm, the participation of even states can be seen as a dip in the strong and broad $n = 1$ peak. Further, they show the peculiar ordering of the states, indicating their interchange. For example, the order of the states for a 29.1 nm thick film is $n = 2, 3, 4, 1, 5$ and 7, which agrees well with the theoretically predicted mode structures shown in figure 3. In this manner, the combination of our theoretical calculations and the non-degenerate two-photon excitation scattering spectroscopy provides a powerful tool to reveal the level structures of confined polaritons in the non-LWA thickness regime. Figure 4(d) shows the transmittance spectrum of the 35.3 nm thick film. From this curve, we understand that even if nonradiative damping is very small, we cannot identify the energy of the polariton eigenstate arising from the $n = 1$ exciton from the linear transmittance.

5. Hyper-parametric scattering in the nano-to-bulk crossover regime

As seen in the previous section, in the non-LWA regime, we can find a peculiar level structure due to the extremely large radiative correction. It is difficult to observe such eigenmodes in the non-LWA regime using linear spectroscopy because of a complicated interference effect between the incident and scattered fields. On the other hand, nonlinear spectroscopies are expected to be useful methods to extract information on eigenmodes because they can avoid the effect of the incident field. In nonlinear spectroscopies, signal weakness in the case of nanoscale samples would be a difficulty. In this section, we propose an additional spectroscopic method providing information on polaritonic eigenmodes in the nano-to-bulk crossover regime by using RHPS.

In RHPS, biexcitons with no angular momentum are coherently excited by two photons, and they collapse by emitting the two photons via polariton states in the medium (see figure 5). Since the emitted photons conserve the wavenumber and energy in the bulk case, they provide information on the dispersion relation of the polaritons [32, 33]. In the case of nanofilms, the wavenumber conservation is no longer valid, and the spectra of RHPS would reflect the energy conservation and level structures of the confined polaritons. By means of this mechanism, we can extract the level structures of the confined polaritons by RHPS. We theoretically demonstrate its possibility in this section. Since the signal photons are generated by a spontaneous emission, the entire description of the motion of signal photons requires a

theoretical framework to treat the EM field quantum mechanically. Thus, in this section, we briefly explain the quantum electrodynamics (QED) version of microscopic nonlocal theory that has been developed by us [31] before the theoretical demonstration of the proposed spectroscopic method.

5.1. QED theory including nonlocal response

Quantization of the electromagnetic (EM) field in condensed matter has been extensively studied. Huttner *et al* [40] performed this work for dispersive and absorptive media, where the EM field includes only the transverse component. Suttorp *et al* have generalized this result by using Laplace transform techniques such that the EM field also includes the longitudinal field in the medium described with the inhomogeneous dielectric functions [41]. We basically adopt the same method as that by Suttorp *et al* to develop the QED theory including the nonlocal effect. We consider the excitonic system to interact with the harmonic oscillators introduced as a heat bath. By assuming that the electromagnetic field interacts with this excitonic system and background absorptive medium, we have derived the equation of motion of the EM field, $\hat{\boldsymbol{E}}^{+}(\boldsymbol{r},\omega)$, from the Heisenberg equation as $[\boldsymbol{\nabla}\times\boldsymbol{\nabla}\times-(\omega/c)^2\epsilon_{\rm b}(\boldsymbol{r},\omega)]\hat{\boldsymbol{E}}^{+}(\boldsymbol{r},\omega) = {\rm i}\mu_0\omega\hat{\boldsymbol{J}}_0(\boldsymbol{r},\omega)+\mu_0\omega^2\hat{\boldsymbol{P}}^{+}_{\rm ex}(\boldsymbol{r},\omega)$, where $\epsilon_{\rm b}(\boldsymbol{r},\omega)$ is the position-dependent background dielectric function; μ_0, the magnetic permeability in vacuum; and $\hat{\boldsymbol{J}}_0(\boldsymbol{r},\omega)$, the noise current density operator. $\hat{\boldsymbol{J}}_0(\boldsymbol{r},\omega)$ is responsible for the fluctuation occurring due to the source of the background EM field and absorption. Similar to reference [41], the expression for $\hat{\boldsymbol{J}}_0(\boldsymbol{r},\omega)$ is derived from the variables included in the original Hamiltonian. It is verified that the same commutation relation holds for $\hat{\boldsymbol{J}}_0(\boldsymbol{r},\omega)$ as that in [41]. By using a Green's function, which is defined by equation (6), this Maxwell equation can be rewritten as

$$\hat{\boldsymbol{E}}^{+}(\boldsymbol{r},\omega)=\hat{\boldsymbol{E}}^{+}_0(\boldsymbol{r},\omega)+\mu_0\omega^2\int {\rm d}\boldsymbol{r}'\,\mathbf{G}(\boldsymbol{r},\boldsymbol{r}',\omega)\cdot\hat{\boldsymbol{P}}^{+}_{\rm ex}(\boldsymbol{r}',\omega), \tag{51}$$

where $\hat{\boldsymbol{E}}^{+}_0(\boldsymbol{r},\omega)$ is the background electric field described by the relation $\hat{\boldsymbol{E}}^{+}_0(\boldsymbol{r},\omega)\equiv {\rm i}\mu_0\omega\int {\rm d}\boldsymbol{r}'\mathbf{G}(\boldsymbol{r},\boldsymbol{r}',\omega)\cdot\hat{\boldsymbol{J}}_0(\boldsymbol{r}',\omega)$. $\mathbf{G}(\boldsymbol{r},\boldsymbol{r}',\omega)$ takes into account the entire geometrical information on the background dielectrics. Regarding the matter system, we consider the excitons and biexcitons with the degrees of freedom of c.m. motions. The Hamiltonian can be expressed as $H_{\rm ex}=\sum_\mu\hbar\omega_\mu b^\dagger_\mu b_\mu+\frac{1}{2}\sum_{\mu,\nu,\mu',\nu'}V_{\rm xx}(\mu;\nu|\mu';\nu')b^\dagger_\mu b^\dagger_\nu b_{\nu'}b_{\mu'}$, where $\hbar\omega_\mu$ and b_μ are the eigenenergy and an annihilation operator of the one-exciton state $|\mu\rangle$, respectively, and $V_{\rm xx}(\mu;\nu|\mu';\nu')$ is the interaction potential that yields the biexciton states. The induced polarization can be expanded using this excitonic basis as $\boldsymbol{P}_{\rm ex}(\boldsymbol{r})=\sum_\mu[\boldsymbol{\mathcal{P}}_\mu(\boldsymbol{r})b_\mu+\boldsymbol{\mathcal{P}}^*_\mu(\boldsymbol{r})b^\dagger_\mu]$, where $\boldsymbol{\mathcal{P}}_\mu(\boldsymbol{r})$ is the expansion coefficient proportional to the c.m. wavefunction. Deriving the Heisenberg equation of excitons, we obtain

$$[\hbar\omega_\mu-\hbar\omega-{\rm i}\gamma_\mu(\omega)/2]\hat{b}_\mu(\omega)=\int {\rm d}\boldsymbol{r}\,\boldsymbol{\mathcal{P}}^*_\mu(\boldsymbol{r})\cdot\hat{\boldsymbol{E}}^{+}(\boldsymbol{r},\omega)+\hat{\mathcal{D}}_\mu(\omega), \tag{52}$$

where $\gamma_\mu(\omega)$ represents the damping constant determined by the coupling strength with the oscillators for heat bath, and $\hat{\mathcal{D}}_\mu(\omega)$ represents the fluctuation due to the coupling with the heat bath, whose commutation relation can be calculated from its explicit expression of it. Substituting the expression of the EM field, equation (51), in this equation, we obtain the self-consistent equation

$$\sum_{\mu'}\left[(\hbar\omega_\mu-\hbar\omega-{\rm i}\gamma_\mu(\omega)/2)\delta_{\mu,\mu'}+\mathcal{A}_{\mu,\mu'}(\omega)\right]\hat{b}_{\mu'}(\omega)=\int {\rm d}\boldsymbol{r}\,\boldsymbol{\mathcal{P}}^*_\mu(\boldsymbol{r})\cdot\hat{\boldsymbol{E}}^{+}_0(\boldsymbol{r},\omega)+\hat{\mathcal{D}}_\mu(\omega) \tag{53}$$

where $\mathcal{A}_{\mu,\mu'} \equiv -\mu_0\omega^2 \int d\boldsymbol{r} \int d\boldsymbol{r}' \, \boldsymbol{\mathcal{P}}^*_\mu(\boldsymbol{r}) \cdot \mathbf{G}(\boldsymbol{r}, \boldsymbol{r}', \omega) \cdot \boldsymbol{\mathcal{P}}_{\mu'}(\boldsymbol{r}')$. This equation is basically the same as equation (9) except for the fluctuation term. In the case of the linear process, the motion of excitons and full EM field are determined by this equation. Since the commutation relations of $\hat{\boldsymbol{J}}_0(\boldsymbol{r}, \omega)$ (and hence $\hat{\boldsymbol{E}}^+_0(\boldsymbol{r}, \omega)$) and $\hat{\mathcal{D}}_\mu(\omega)$ are known, we can calculate them for $\hat{\boldsymbol{E}}^+(\boldsymbol{r}, \omega)$ and $\hat{b}_\mu(\omega)$.

If we include the Heisenberg equation of biexcitons into the self-consistent equation set, the following term is added to the right-hand side of equation (53): $\sum_{\lambda,\nu}(\hbar\omega_\mu + \hbar\omega_\nu - \hbar\Omega_\lambda) F_{\lambda,\mu,\nu} \int_{-\infty}^{\infty} d\omega' \, b^\dagger_\nu(\omega - \omega')\hat{B}_\lambda(\omega')$, where $\hat{B}_\lambda(\omega)$ and $\hbar\Omega_\lambda$ are the amplitude and eigenenergy of biexcitons, respectively, and $F_{\lambda,\mu,\nu}$ is the coefficient obtained when we expand the biexcitonic states as $|\lambda\rangle = \frac{1}{2}\sum_{\mu,\nu} F_{\lambda,\mu,\nu} b^\dagger_\mu b^\dagger_\nu |g\rangle$. The selection rules for the two-photon absorption and scattering are determined by this biexcitonic wavefunction. Instead of a complete self-consistent handling of this nonlinear equation, we replace $\hat{B}_\lambda(\omega)$ by its average $\langle\hat{B}_\lambda(\omega)\rangle$ assuming a sufficiently strong classical incident field with no quantum fluctuation and no higher-order nonlinearity. With regard to $F_{\lambda,\mu,\nu}$, we formulate this wavefunction by considering the model of the lowest state of the biexcitonic relative motion including an effective volume as the fitting parameter [32]; this is a reasonable treatment that focuses on the effects of the degree of freedom of the excitonic (biexcitonic) c.m. motion. By introducing phenomenological damping in the biexciton, we can solve the above-mentioned self-consistent equations, which enables us to calculate $\hat{\boldsymbol{E}}^+(\boldsymbol{r}, \omega)$ through equation (51).

5.2. RHPS in the nano-to-bulk crossover regime

Using the same excitonic model as in the previous section, we calculate the RHPS spectra obtained from CuCl films. We assume the binding energy of biexcitons (b_x) and the absorption width of excitons to be 32.2 and 0.1 meV, respectively.

Now, we assume an experimental scheme with the pump–probe-type measurement; namely, we excite a certain excitonic state by a pump beam and sweep a probe beam energy. The results are shown in figure 6, where the same excitonic parameters as those in figure 2 are used. The emitted photon pairs satisfy the conservation of $\boldsymbol{K}_\parallel$ and energy. In the case of the normal incidence, for example, respective photons in a pair have $\boldsymbol{K}_\parallel$ with the same magnitude and opposite signs. The same spectra are obtained in the two detectors for $\boldsymbol{K}_\parallel$ and $-\boldsymbol{K}_\parallel$ if we scan in the same energy range for the respective detectors. Figure 6(c) shows the scattering intensity as a function of the probe energy and the energy of an emitted photon. The pumped polariton level is chosen so that the strongest signal is obtained. This figure provides information on the energy levels of the confined biexcitons and excitons. In figure 6(c), we can see several peaks by scanning the energy on the probe energy axis. If the total energy of the pump and probe energies coincides with a quantized biexciton energy, the signal is resonantly enhanced. Thus, these peaks provide information on biexciton levels. On the other hand, a particular state of the biexciton tends to be selectively connected with a particular polariton state having the same parity. This is why the peak positions on the lines of the respective biexciton levels slightly shift to the upper energy side with an increase in the biexciton level. These peak structures reflect the level scheme of the confined polaritons (see figure 6(b)).

In the actual experiments, it might not be easy to sweep the probe energy. Instead, irradiating using a probe pulse with a wide line width might be feasible. In this case, several states of confined biexcitons contribute to the RHPS signal at the same time because of the wide range excitation. Figure 6(a) shows the spectrum corresponding to this case where we perform an integration over the probe energy. Although the information on the biexciton levels is lost, the polariton level structure reflecting their eigenenergies and widths can be obtained even in this case (compare figure 6(a) with (b)). Figures 6(d)–(f) show the thicker case (150 nm),

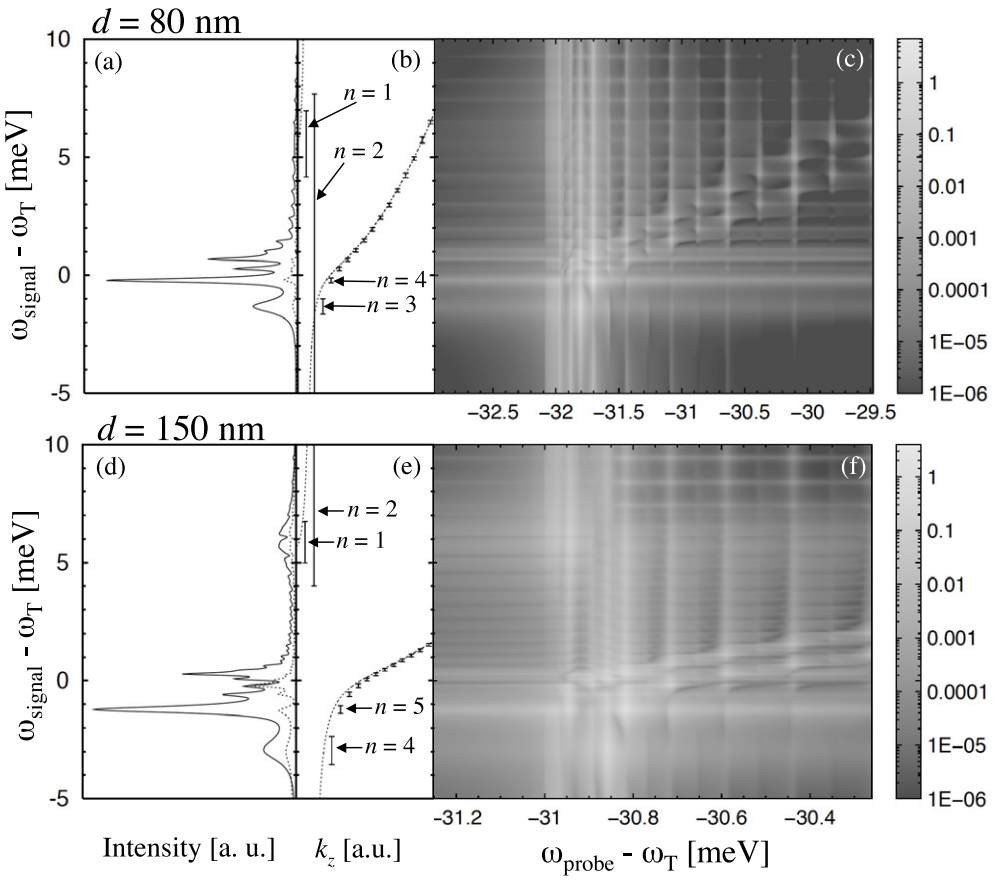

Figure 6. Scattering intensity of RHPS. (a) and (d) Probe-energy integrated intensity ($\theta = 0$). Solid and dotted lines are obtained by the induced and degenerate two-photon excitations, respectively. The latter curve is multiplied by 10; the former intensity is much larger than that of the latter. In the case of induced excitation, $n = 4$ and 5 polaritons are pumped for (a) and (d), respectively. (b) and (e) Dispersion relation of exciton polaritons confined in the film. The positions of vertical bars in (b) and (e) indicate eigenenergies of confined polaritons including the radiative shift. The lengths of these bars indicate the sum of the radiative and absorption widths of the confined-polariton states. n denotes the quantum number of the original excitonic state of each polariton. In (e), the $n = 3$ state is out of the displayed energy range. (c) and (f) Probe-energy resolved intensity.

where the polariton level structures reflecting much larger radiative corrections can be observed. Further, in figures 6(a) and (d), we can see how the signal by the non-degenerate induced excitation is enhanced from that by the degenerate two-photon excitation. For the present value of the damping constant, the signal of the non-degenerate induced excitation is larger than that of the degenerate two-photon excitation by approximately two orders of magnitude.

In the case of even thicker films, there is a possibility that the damping effect hinders the efficient generation of the RHPS signal. However, if we select appropriate states for pumping, we can obtain a sufficiently strong signal due to multiple enhancement. Figure 7 shows the spectrum for $d = 412$ nm obtained by the pumping of the $n = 1$ polariton. In the case of this thickness, the $n = 1$ polariton is located immediately above the longitudinal exciton energy ω_L due to the large positive radiative shift, and it strongly enhances the internal field in this thickness region (factor 1). Interestingly, in the case of this thickness, there exists

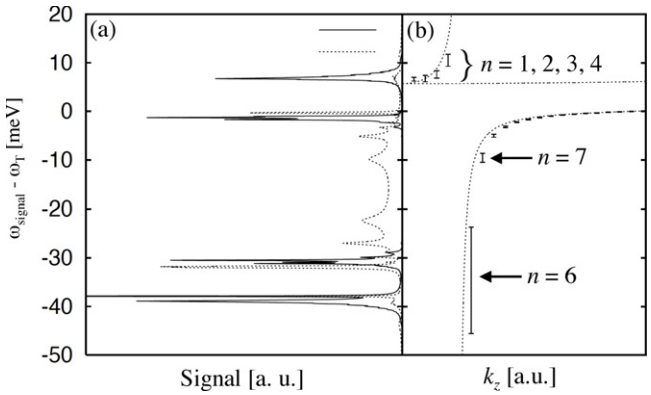

Figure 7. Scattering intensity of RHPS. (a) Probe-energy integrated intensity ($\theta = 60°$). Solid and dotted lines are obtained by the induced excitation and the degenerate two-photon excitation, respectively. The latter is multiplied by 10. (b) Dispersion relation of exciton polaritons confined in the film. The meanings of the vertical bars and n are the same as in figure 6.

a polariton state ($n = 6$), which shifts to the lowest energy side reaching an energy level that coincides approximately with the transition energy between the pumped polariton state and a particular ($m = 6$) biexciton state (see figure 7(b)). This double resonance condition strengthens the biexciton relaxation (factor 2). The two types of factors (1 and 2) cause a multiplier enhancement of the signal intensity; as a result, the efficiency is similar to that of the bulk case.

In this way, RHPS by non-degenerate induced excitation provides signals that are sufficiently strong to be detected, and they include rich information on the level structures of confined biexcitons and polaritons in the nano-to-bulk crossover regime.

6. Summary and future prospects

In this article, we have discussed exciton–radiation coupling in the sample-size regime beyond the long-wavelength approximation (LWA). In high-quality samples, the excitonic coherence can be considerably long, and recent fabrication technologies provide matter systems where the interplay between the spatial structures of the radiation wave and excitonic wave plays an essential role. After providing an overview of the background and recent theoretical and experimental works related to the optical responses that are peculiar to this size regime, we introduced a theoretical framework to treat the optical response in the non-LWA regime. Further, we presented the calculated results showing the anomalous level structure of the exciton–radiation coupled system (polaritons) in a thin film. The eigenenergies of the confined polaritons generally include radiative shift and width. In the non-LWA regime, this radiative correction becomes extremely large, which leads to peculiar properties of polaritons, such as the size-resonant enhancement of the radiative damping constant, and successive interchanges of the quantum states.

In order to reveal the level structure of the polaritons in the non-LWA regime, we presented a method based on the combination of the experiment with non-degenerate two-photon excitation scattering spectroscopy and the corresponding theoretical analysis with the nonlocal theory for the second-order nonlinear process. This method has enabled successful observation of the signal of confined polaritons in a thin film in the non-LWA regime, and the interchange of confined polariton states has been elucidated. Further, the theoretical analysis

beautifully explains the observed spectra, which establishes the predicted level structure of the confined polaritons.

As another method to study the confined polaritons in the non-LWA regime, we proposed a resonant hyper-parametric scattering (RHPS) spectroscopy with a non-degenerate induced excitation. Since the signal photons are generated through spontaneous emission from biexcitons, a complete description of the motion of signal photons requires a theoretical framework to treat an electromagnetic (EM) field quantum mechanically. After a brief explanation of the quantum electrodynamics (QED) version of the microscopic nonlocal theory developed by us [31], we demonstrated some calculations for thin films in the nano-to-bulk crossover regime. As a result, it was shown that this method provides rich information on the confined biexcitons and polaritons.

In the conventional theory of optical response, the oscillator strength is a standard measure of the radiation–matter coupling, where the LWA is a basis for this framework. The scale of the radiation wavelength is normally different from that of the matter wavelength. Therefore, the situation where the interplay between these waves plays an essential role has not been in the spotlight so far. However, the recent progress in the theory, fabrication technologies, and spectroscopic techniques have led to new fields being established. In other words, we now understand that the long-range coherence of the confined excitons and non-LWA effects cause the anomalous level structure of polaritons, which leads to new types of optical phenomena that are peculiar to the nano-to-bulk crossover regime. (Or, interesting phenomena might have been hindered or overlooked so far because of the lack of dependable theoretical methods and fabrication technologies to realize a long-range excitonic coherence.) It should be remarked that the proposed effects presented here are not peculiar to a particular material system. Therefore, further similar studies for materials other than CuCl, such as ZnO and GaN, would lead to a new search space for novel photo-functions in the non-LWA regime. Further, the interplay between the radiation and matter waves would emerge not only through the optical response but also through chemical reaction or mechanical interaction of small objects [42, 43]. We hope that the study to fully reveal such potentiality of the nano-to-bulk crossover regime will be continued.

Acknowledgments

The authors are grateful to Professor K Cho for his fruitful discussions and support. They also thank Dr H Ajiki for his useful discussions, and Dr B P Zhang for his collaboration in the experiments, and Mr K Sugihara and Mr J Kishimoto for their collaboration during theoretical studies. This work was partially supported by a Grant-in-Aid for Creative Scientific Research (17GS1204) from the Japan Society for the Promotion of Science.

References

[1] Takagahara T 1987 *Phys. Rev.* B **36** 9293
[2] Kayanuma Y 1988 *Phys. Rev.* B **38** 9797
[3] Hanamura E 1988 *Phys. Rev.* B **37** 1273
[4] Takagahara T 1989 *Phys. Rev.* B **39** 10206
[5] Rashba E I and Gurgenishvili G E 1962 *Fiz. Tverd. Tela (Leningrad)* **4** 1029
Rashba E I and Gurgenishvili G E 1962 *Sov. Phys.—Solid State* **4** 759 (Engl. Transl.)
[6] Henry C H and Nassau K 1970 *Phys. Rev.* B **1** 1628
[7] Tang Z K, Yanase A, Yasui T, Segawa Y and Cho K 1993 *Phys. Rev. Lett.* **71** 1431
[8] Masumoto Y, Yamazaki M and Sugawara H 1988 *Appl. Phys. Lett.* **53** 1527
[9] Itho T, Jin F and Ikehara T 1989 *Nonlinear Optics of Organics and Semiconductors* (*Proceedings in Physics* vol 36) ed T Kobayashi (Berlin: Springer) p 76

[10] Nakamura A, Yamada H and Tokizaki T 1989 *Phys. Rev.* B **40** 8585
[11] Kiselev V A, Razbirin B S and Uraltsev I N 1975 *Phys. Status Solidi* b **72** 161
[12] Mita T and Nagasawa N 1982 *Solid State Commun.* **44** 1003
[13] Cho K and Kawata M 1985 *J. Phys. Soc. Japan* **54** 4431
[14] Cho K, D'Andrea A, Del Sole R and Ishihara H 1990 *J. Phys. Soc. Japan* **59** 1853
[15] Tang Z K, Yanase A, Segawa Y, Matsuura N and Cho K 1995 *Phys. Rev.* B **52** 2640
[16] Ishihara H and Cho K 1992 *Proc. Int. Symp. on Science and Technology of Mesoscopic Structures (Nara, 1991)* ed S Namba, C Hamaguchi and T Ando (Berlin: Springer) pp 464–9
[17] Ishihara H and Cho K 1993 *Phys. Rev.* B **48** 7960
[18] Ishihara H and Cho K 1996 *Phys. Rev.* B **53** 15823
[19] Ishihara H, Amakata T and Cho K 2002 *Phys. Rev.* B **65** 035305
[20] Akiyama K, Tomita N, Nomura Y and Isu T 1999 *Appl. Phys. Lett.* **75** 475
[21] Ishihara H, Cho K, Akiyama K, Tomita N, Nomura Y and Isu T 2002 *Phys. Rev. Lett.* **89** 017402
[22] Ishihara H, Cho K, Akiyama K, Tomita N and Isu T 2002 *Phys. Status Solidi* a **190** 849
[23] Cho K 1991 *Prog. Theor. Phys. Suppl.* **106** 225
[24] Cho K 2003 *Optical Response of Nanostructures: Microscopic Nonlocal Theory* (Berlin: Springer)
[25] Ishihara H, Asakawa H and Cho K 2000 *Physica* E **7** 671
[26] Ajiki H, Tsuji T, Kawano K and Cho K 2002 *Phys. Rev.* B **66** 245322
[27] Ishihara H, Kishimoto J and Sugihara K 2004 *J. Lumin.* **108** 342
[28] Ishihara H 2002 *Nonlinear Opt.* **29** 663
[29] Syouji A, Zhang B P, Segawa Y, Kishimoto J, Ishihara H and Cho K 2004 *Phys. Rev. Lett.* **92** 257401
[30] Ichimiya M, Ashida M, Yasuda H, Ishihara H and Itoh T 2006 *Phys. Status Solidi* b **243** 3800
[31] Bamba M and Ishihara H 2006 *Phys. Status Solidi* c **3** 3460
[32] Ueta M, Kanzaki H, Kobayashi K, Toyozawa Y and Hanamura E 1986 *Excitonic Processes in Solids* (Berlin: Springer)
[33] Itoh T and Suzuki T 1978 *J. Phys. Soc. Japan* **45** 1939
[34] Savasta S, Marino G and Girlanda R 1999 *Solid State Commun.* **111** 495
[35] Edamatsu K, Oohata G, Shimizu R and Itoh T 2004 *Nature* **431** 167
[36] Chew W C 1990 *Waves and Fields in Inhomogeneous Media* (Princeton, NJ: Van Nostrand Reinhold)
[37] Itoh T, Katohno T, Kirihara T and Ueta M 1984 *J. Phys. Soc. Japan* **53** 854
[38] Mita T, Sotome K and Ueta M 1980 *J. Phys. Soc. Japan* **48** 496
[39] Feldman A and Horowitz D 1969 *J. Opt. Soc. Am.* **59** 1406
[40] Huttner B and Barnett S M 1992 *Phys. Rev.* A **46** 4306
[41] Suttorp L G and Wubs M 2004 *Phys. Rev.* A **70** 013816
[42] Iida T and Ishihara H 2003 *Phys. Rev. Lett.* **90** 057403
[43] Iida T and Ishihara H 2006 *Phys. Rev. Lett.* **97** 117402